Superior Capacitive Energy-Storage Performance in Pb-Free Relaxors with a Simple Chemical Composition

Zheng Sun[1,2,#], Huajie Luo[1,3,#], Yonghao Yao[1,3], Na Wang[1,3], Liang Chen[1,3], Tianyu Li[1,3], Changzheng Hu[7], He Qi[1,3], Shiqing Deng[1,2], Ji Zhang[4,*], Leighanne C. Gallington[6], Yuanpeng Zhang[5], Joerg C. Neuefeind[5], Hui Liu[1,2,*], and Jun Chen[1,2,3,*]

[1]Beijing Advanced Innovation Center for Materials Genome Engineering, University of Science and Technology Beijing, Beijing 100083, China

[2]School of Mathematics and Physics, University of Science and Technology Beijing, Beijing 100083, China

[3]Department of Physical Chemistry, University of Science and Technology Beijing, Beijing 100083, China

[4]School of Materials Science and Engineering, Nanjing University of Science and Technology, Nanjing, Jiangsu 210094, China

[5]Chemical and Engineering Materials Division, Oak Ridge National Laboratory, Oak Ridge, Tennessee 37831, USA

[6]X-ray Science Division, Argonne National Laboratory, Lemont, Illinois 60439, USA

[7]College of Materials Science and Engineering, Guilin University of Technology, Guilin 541004, China

[#]Zheng Sun and Huajie Luo contribute equally to this work.

*Corresponding author. huiliu@ustb.edu.cn, jizhang@njust.edu.cn, and junchen@ustb.edu.cn

Abstract

Chemical design of lead-free relaxors with simultaneously high energy density (W_{rec}) and high efficiency (η) for capacitive energy storage has been a big challenge for advanced electronic systems. The current situation indicates that realizing such superior energy storage properties requires very complex chemical components. Herein, we demonstrate that, via local structure design, ultrahigh W_{rec} of 10.1 J/cm^3, concurrent with high η of 90%, as well as excellent thermal and frequency stabilities can be achieved in a relaxor with very simple chemical composition. By introducing $6s^2$ lone

pair stereochemical active Bi into the classical $BaTiO_3$ ferroelectric to generate a mismatch between *A*- and *B*-site polar displacements, a relaxor state with strong local polar fluctuations can be formed. Through advanced atomic-resolution polar mapping, and 3D reconstructing nanoscale structure from neutron/X-ray total scattering, it is revealed that the localized Bi enhances the polar length largely at several perovskite unit-cells and disrupt the coherent Ti polar displacement, resulting in a slush-like structure with extremely small size polar clusters and strong local polar fluctuations. This favorable relaxor state exhibits substantially enhanced polarization, and minimized hysteresis at high breakdown strength. This work offers a feasible avenue to chemical designing new relaxors with simple composition for high-performance capacitive energy storage.

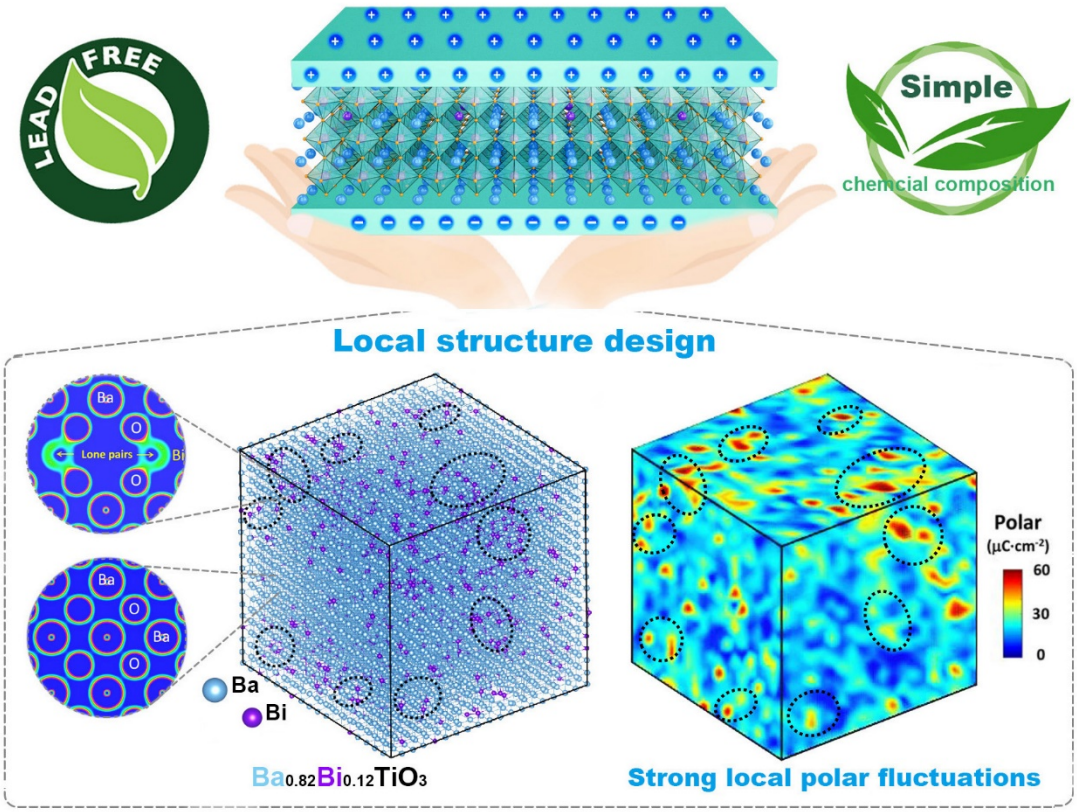

Introduction

With the rapidly growing field of renewable energy production, automotive electrification and portable electronics, there is an urgent need for efficient, environmentally-friendly and cost-effective electrical energy storage devices[1-6]. Dielectric capacitors store electrical energy as the electrostatic field, showing the highest power density, fastest charging/discharging capability along with superior cyclability and highest operating voltage among currently available energy storage devices, and playing an indispensable role in modern electrical and electronic systems[7-9]. However, their applications are limited due to low energy density compared with electrochemical energy storage devices. Further, high energy efficiency is pursued to minimize energy dissipation and ensure reliability. Therefore, ever-increasing efforts have been dedicated to enhancing recoverable energy density (W_{rec}) and efficiency (η) to meet the persisting demand for miniaturization, integration, and compactness of eco-friendly advanced devices[10-12].

In the past five years, plenty of lead-free perovskite-type compounds have been developed for capacitive energy storage. Yet, most of these ceramics present W_{rec} below 5 J/cm^3, η below 80% (Fig. S1). Recently, record-high W_{rec} of 7.01, and 15.9 J/cm^3 has been achieved in $AgNbO_3$-based[13], and $BiFeO_3$-based bulk ceramics[14], respectively, while all of them possess η lower than 90%. Although high η can be achieved in some $BaTiO_3$ (BT) -based, $SrTiO_3$ (ST) -based and $Bi_{0.5}Na_{0.5}TiO_3$ (BNT) -based relaxor ceramics, their corresponding W_{rec} are relatively low (about 4-6 J/cm^3)[15-17]. It seems that the improvement of energy density is typically accompanied by the deterioration in efficiency, and vice versa. Achieving ultrahigh energy storage density ($W_{rec} \geq 10$ J/cm^3) with ultrahigh efficiency ($\eta \geq 90\%$) in lead-free ceramics remains a challenge.

Relaxors have shown great promise for superior energy storage performance, due to the slim hysteresis with small remnant polarization (P_r). Chemical design is the most prevailing method to develop relaxors with enhanced energy storage properties. Based on rational chemical element substitution/doping and constructing solid-solutions, various strategies, such as domain modification[18,19], superparaelectric state[1,20,21], high-

entropy[22], phase structure control[23-26], have been proposed. Furthermore, breakdown strength (E_b) is also an important parameter, and can be improved through nanostructure construction [27,28], grain refining[29], and defect engineering[30] etc. With synergistic combinations of these strategies, great advances have been achieved, for instance, the realization of W_{rec} > 10 J/cm^3 and η > 90% in two very complex KNN-based high-entropy[22] and (Na,K)(Sb,Nb)O_3-$SrZrO_3$-($Bi_{0.5}Na_{0.5}$)ZrO_3[21] relaxor bulk ceramics. The energy storage performance in relaxors has progressively improved, yet, it is accompanied by more and more complex chemical compositions. It appears that complex chemical composition is required for attaining excellent energy storage performance. Actually, for industrial production, the material with complex chemical composition is no doubt unfavorable, which will reduce the manufacturing efficiency, increase the cost, and influence the process stability. Hence, question emerges, can superior energy storage performance be achieved in relaxors with simple chemical composition?

To achieve high W_{rec} and η simultaneously, we propose designing relaxor with "strong local polar fluctuations". BT-based materials are the most widely used type of dielectric ceramic capacitors[31], and serve as a model system in this study. BT is a classic ferroelectric, presenting a distinctive structure features that long-range *R*, *O*, and *T* can occur at different temperatures. It is known that the long-range polar order in BT is driven by *B*-site. As shown by the DFT calculations (Fig. 1a), the interaction between Ba and O is completely ionic in BT; while, when introducing strong ferroelectric active Bi, large polar displacement can be formed due to the strong hybridization between the stereochemical Bi 6s^2 lone pairs and O 2*p* orbitals. Simultaneously, the long-range polar order in BT will be broken, forming local *R*, *O*, *T* or lower symmetry polar clusters due to the mismatch between Bi and Ti polar displacements, and therefore generating strong local polar fluctuations (Fig. 1b and 1c). Such polar structure feature will manifest slim hysteresis with significantly enhanced maximum polarization (P_m) and reduced remnant polarization (P_r), and thus achieving W_{rec} and η simultaneously (Fig. 1d).

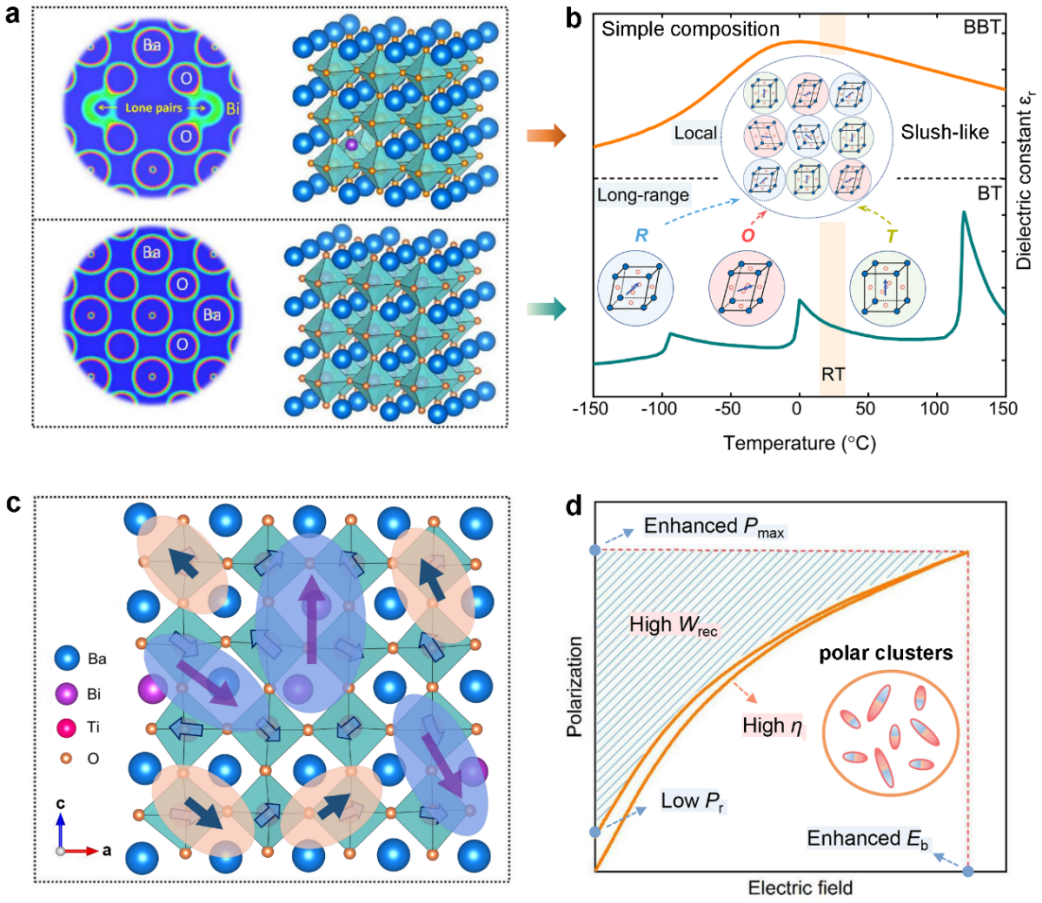

Figure 1. Schematic diagram of design local structure with strong local polar fluctuations to achieve superior energy storage performance. (a) Electron localization function on *A*-O plane of BBT and BT from the DFT calculations. (b) Transforming from long-rang polar order ferroelectric state into relaxor state with multiple local symmetries polar clusters. (c) The mismatch between Bi and Ti polar displacements leads to strong local polar fluctuations. (d) Illustration of polarization loop with enhanced maximum polarization P_m, reduced remnant polarization P_r, and improved breakdown strength E_b.

Herein, by local structure design that simply introduces strong ferroelectric active Bi into the classical $BaTiO_3$, we obtain superior energy storage performance. It is found that the localized Bi regions present largely enhanced polar length at a few unit-cells and break the Ti-driven long-range polar order, thus forming multiple local symmetries polar clusters with extremely small sizes and strong local fluctuation. The favorable relaxor state exhibits large P_m and suppressed P_r, along with the enhanced breakdown

strength, and giving rise to a giant W_{rec} of 10.1 J/cm^3 with high η of 90%.

Results and discussion

$Ba_{1-1.5x}Bi_xTiO_3$ ($0 \le x \le 0.14$) solid solutions were explored to optimize the composition. As indicated by the XRD patterns (Figs. S2(a-b)), the Bi can be completely diffused into $BaTiO_3$ lattice matrix and form a pure perovskite phase when $x \le 0.12$. With increasing x, the long-range structure changes from tetragonal to pseudo-cubic, indicating that the introduction of strong ferroelectric active Bi into the *A*-site gradually breaks the *B*-site-driven long-range ferroelectric order. Correspondingly, the hysteresis loop evolves from typical ferroelectric loops into slim loops (Fig. S2c), indicating the transformation from ferroelectric to relaxor ferroelectric state. Particularly, $Ba_{0.82}Bi_{0.12}TiO_3$ (BBT12) presents extremely slim loops with negligible hysteresis and near-zero P_r, suggesting the high η for capacitive energy storage. Interestingly, the relaxor state of BBT12 shows very strong dielectric relaxation behavior (Fig. S3). The frequency-dependent shift in T_{max}, defined as $\Delta T_{max} = T_{max}(10^6\ \text{Hz}) - T_{max}(10^3\ \text{Hz})$, is as high as 75 K. This value is much higher than the classical relaxors, such as PMN (20 K)[32], $Ba(Ti,Zr)O_3$ (~ 25 K)[33], suggesting the existence of extremely small polar entireties in BBT12. Considering the *P*-*E* loops observed low at electric field and the dielectric relaxor behavior of BBT system, the optimal composition for excellent energy storage performance will be BBT12, thus its microstructure is studied subsequently.

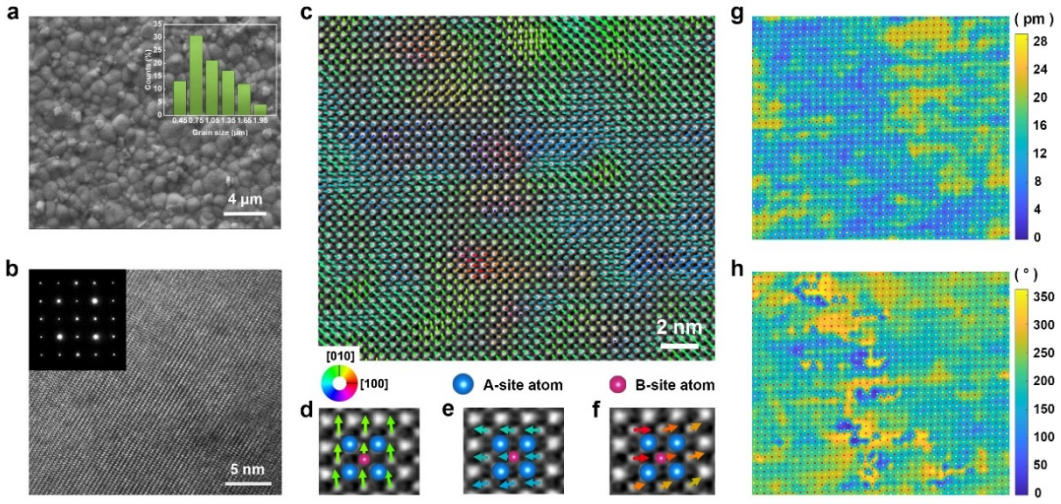

Figure 2. Microstructure of BBT12 revealed by electron microscopes. (a) SEM image of ceramic. The inset indicates the statistical analysis of the grain size distribution. (b) High-resolution bright-field image and corresponding electron-diffraction pattern along $[001]_c$. (c) Atomic resolution polar vectors mapping according to the HAADF STEM image recorded along the $[001]_c$. (d-f) Enlarged images of representative areas from (c), the positions of the *A*- and *B*-site atomic columns and corresponding *B*-site cation displacement vectors in each unit cell are indicated. (g) Polar magnitude mapping, and (h) polar angle mapping along the $[001]_c$.

BBT12 ceramics were sintered well with fine grains (about 1 μm) and high density (about 96% of theoretical density) (Fig. 2a). Similar to classical relaxors, BBT12 exhibits long-range average cubic structure, as detected from the electron diffraction patterns along the $[001]_c$ zone. No long-range ferroelectric domains but instead a light and shade contrast occurs (Fig. 2b). It is known that different energy storage performance can be obtained in relaxors with different compositions. While from the long-range average structure point of view, they present cubic structure, and thus cannot interpret the different polarization loops. The prominent features of relaxors are compositional heterogeneity-driven heterogeneous polar structures. Therefore, aberration-corrected scanning transmission electron microscopy (STEM) was employed to directly observe the atomic-level polar structures. The STEM HAADF (high angle annular dark field) atom images were obtained from $[100]_c$ zone axis (Fig. 2c and Fig. S4). The positions of the *A*-site (Bi/Ba with stronger intensity contrast) and *B*-site (Ti with weaker intensity contrast) atomic columns have been estimated by Gaussian fitting, and are indicated in the enlarged images on Figs. 2(d-f). The polar displacement vectors including the magnitude and orientation can be measured as the deviation of the position of *B* sites atom relative to the center of its four nearest neighboring *A*-site positions. Figs. 2(c-h) show the polar polar displacement mapping according to the atomic-resolution TEM images. About 1-3 nm large polar clusters is observed. Interestingly, these polar clusters are not isolated from neighbouring clusters by the non-polar matrix, but being connected by polar matrixes with smaller but

detectable polar displacements. Multiple local symmetries including *T*, *R*, *O* and *M* (monoclinic) or possibly lower symmetry polar clusters occur, and forming a gradual transition between different clusters. It demonstrates that BBT12 relaxor resembles as a slush-like polar structure[34]. The longest arrows identified for a displacement is about 28 pm and average displacement is about 15 pm. These values are much larger than the (Ba,Sr)TiO_3 and $BaTiO_3$[35], and confirming that the introduction of Bi increases the local polar length. The unique features of large local polar length and extremely small size result in strong local polar fluctuation. Such a relaxor state can be reflected from the remarkably enhanced ΔT_{max} observed in the dielectric spectrum (Fig. S3). It is widely recognized that small polar clusters can energetic response to external electric field, and thus leading to low loss and high thermal breakdown strength.

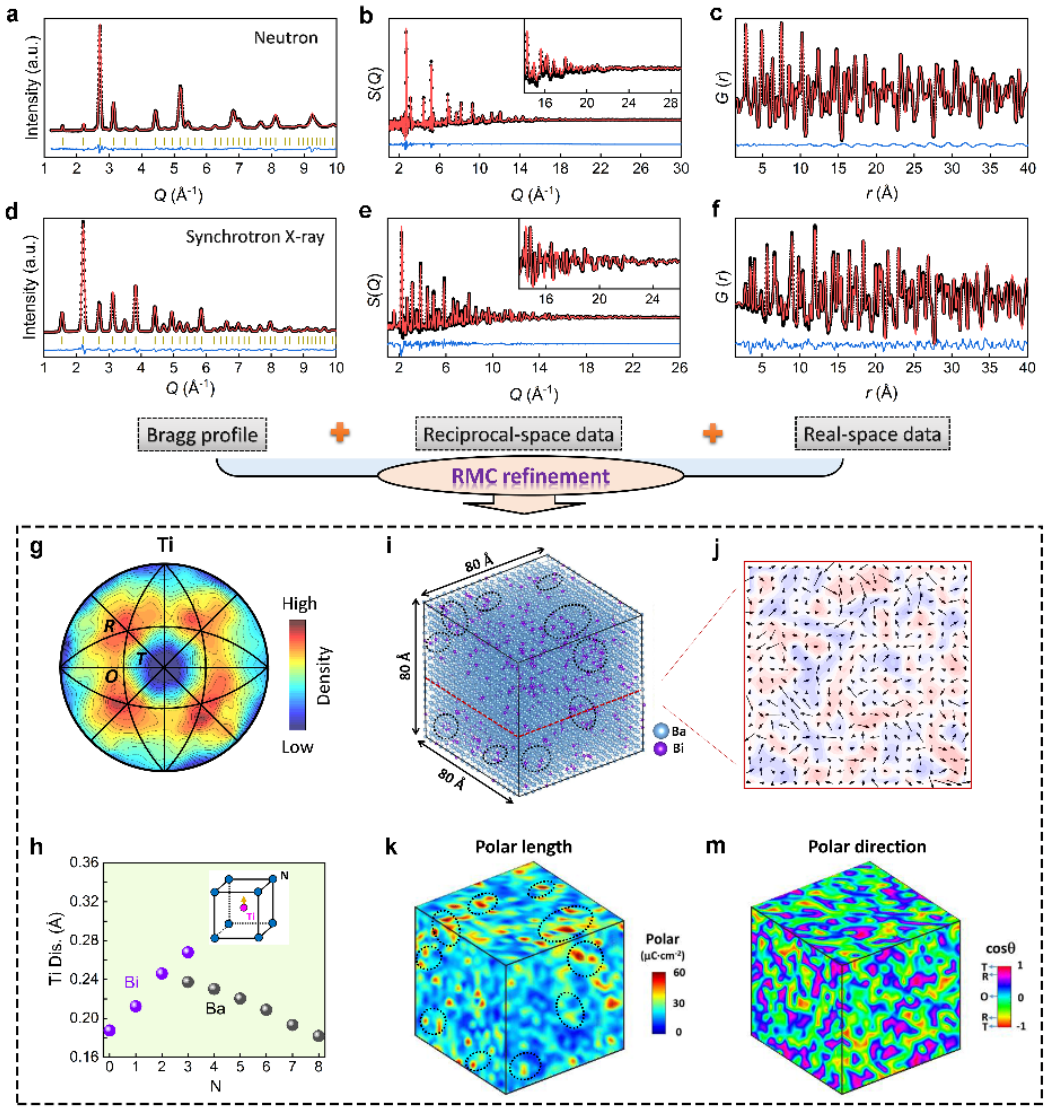

Figure 3. Constructing 3D atomic configuration and corresponding local polar distribution by fitting neutron and X-ray real space PDF data, reciprocal-space $S(Q)$ data and Bragg profiles through reverse Monte Carlo algorithm of BBT12. (a-f) Fitting results of neutron-based, X-ray-based PDF $G(r)$, $S(Q)$, and Bragg profile. The black point, red line, and the blue line indicate the measured data, calculated data, and residual curves. (g) Stereographic projections of Ti polar displacements viewing along $[001]_c$, (h) Magnitudes of Ti polar displacements as a function of the number of Bi and Ba in $[A_8Ti]$ clusters, (i) 3D distribution of A site atoms, (j) 2D polar distribution extracted from the marked slice. (k) and (m) Corresponding 3D distribution of magnitude and direction of polar vector in figure i, respectively.

The atomic-resolution polar mapping gives the direct 2D local polar distribution, but cannot provide the relation between local chemical inhomogeneity and local polar inhomogeneity. Interestingly, the atomic pair distribution function (PDF) based on total scattering is a tool that can go beyond conventional diffraction analysis and offer quantitative information about local and sub-nanoscale structures[36,37]. The new advances in big-box structure-refinement methodology enable to establish 3D atomic configuration directly by fitting the experimental total scattering data[38,39]. To construct the 3D nanoscale structure of BBT12, both neutron and X-ray total scattering data were collected. A big-box atomic configuration with 20 × 20 × 20 perovskite unit cells (40000 atoms, approximately 80 × 80 × 80 $Å^3$) was refined according to an RMC algorithm by simultaneously fitting six experimental data, including neutron-based and X-ray-based reciprocal-space $S(Q)$ data and real-space PDF $G(r)$ data, and Bragg profiles. As shown in Fig. 3, six data can be fitted well, for example, the long-range cubic structure shown in the Bragg profile (Figs. 3a and 3d), and the evident asymmetry of the nearest Ti-O atomic pair in the PDF $G(r)$ (Fig. S5).

As is widely known, the long-range polar order in canonical $BaTiO_3$ is driven by *B*-site of Ti. Based on recent results, although $BaTiO_3$ exhibits long-range *R*, *O* and *T* at different temperatures, the local Ti is displaced along the $[111]_c$ direction in these structures. To reveal the influence of the introduced Bi on the local Ti polar

displacement, the D_{Ti} vector was first extracted from the refined atomic configuration. Locally, the Ti is displaced preferentially along eight $[111]_c$ directions with strong diffusion that covers *M*, *O* and *T*, which is much more diffused compared with parent *T* phase $BaTiO_3$ (Fig. S6). The local *A*-site chemistry will affect AO_{12} octahedral distortions, and thus influences the Ti polar displacement. As shown in Fig. 3h, the number of Bi in the $[A_8Ti]$ cluster is directly affects the Ti displacement. For the $[A_8Ti]$ clusters with Bi number increasing from 0 to 3, the average D_{Ti} increases from 0.17 Å to 0.28 Å. On the other hand, the opposite trend occurs with respect to the local Ba content in the $[A_8Ti]$ cluster. The localized Bi significantly enhances the local polar displacements.

For perovskite-structured compounds, the polar is not only from the *A* site but also from the *B* site. Therefore, the 3D atomic configuration and corresponding polar vectors were established for the *B* site as well. As shown in Fig. 3i, the Bi is randomly distributed in the Ba matrix, which agrees well with the element mapping results from electron microscope (Fig. S7). Polar clusters occur with size about 3-5 unit-cells. Particularly, polymorphic *R*, *T*, *O*, *M* and lower symmetry clusters exist. Notably, no non-polar matrix instead disorder polar region is observed. The whole structure rather resembles a slush-like structure, in which clusters interplay directly with each other. The extracted representative 2D polar map from 3D atomic reconstruction is consistent well with the polar mapping from atomic-resolution TEM images (Fig. 2). Specifically, the Bi rich regions present much larger local polar length, where the polar length is estimated to be about 50-60 $\mu C/cm^2$, more than twice that in the parent $BaTiO_3$ (about 25 $\mu C/cm^2$). Simultaneously, the randomly distributed Bi destroys the coherent Ti polar displacements, leading to strong local polar fluctuations. Notably, the enhanced relaxor feature of polymorphic symmetry polar clusters has been designed for capacitive energy storage by introducing several chemical components, such as BF-ST-BT ternary system[18], high-entropy KNN-based[19,22] etc. In this study, such polar structure is obtained by simply introducing Bi in $BaTiO_3$. In a word, the experimental results were in good accordance with our design. The slush-like structure with extremely small polar

clusters and strong local polar fluctuations in BBT12 implies a superior energy storage performance.

Benefiting from the unique local structure, BBT12 ceramic presents superior energy storage performance (Fig. 4). The parent $BaTiO_3$ possesses a relatively low P_m =19.7 μC/cm^2, relatively high P_r =6.3 μC/cm^2, at a low E_b =8 kV/mm (Fig. S8), giving rise to an inferior energy storage performance (W_{rec} =0.05 J/cm^3, η =57.8%). This is hindered by the long-range polar order and small intrinsic polar length. After local structure design with strong local polar fluctuations, a slim *P-E* loop with a large P_m of 48 μC/cm^2, and suppressed P_r of 6 μC/cm^2, can be achieved at a high E_b of 70 kV/mm in BBT12 ceramic. Interestingly, an ultrahigh W_{rec} 10.1 J/cm^3 accompanied by η of 90% is obtained. As a comparison, BBT12 ceramic present the record-high W_{rec} among all reported BT-based ceramics. Further, BBT12 ceramic shows high W_{rec} when compared with all these η > 90%. Very recently, superior performance of W_{rec} > 10.1 J/cm^3 and η > 90% have achieved in two lead-free systems, KNN-based[22] high-entropy and $(Na,K)(Sb,Nb)O_3$–$SrZrO_3$–$(Bi_{0.5}Na_{0.5})ZrO_3$[21] relaxor, but both have very complex chemical composition. As shown in Fig 4e and 4f, it appears that enhancing W_{rec} in lead-free ferroelectric relaxors requires the collaborative introduction of multi-components[14,22,21,40]. However, a material with complex chemical composition is not conducive to large-scale production. The realization of high W_{rec} and high η in BBT with very simple chemical compositions breaks through the current situation where high energy storage performance requires very complex chemical components. Given the fact that BT-based ceramics are mainstays as dielectric capacitors in the industry with mature technology and relatively low cost. It is expected that the BBT may become one of the lead-free dielectric capacitors and a promising candidate for energy storage applications.

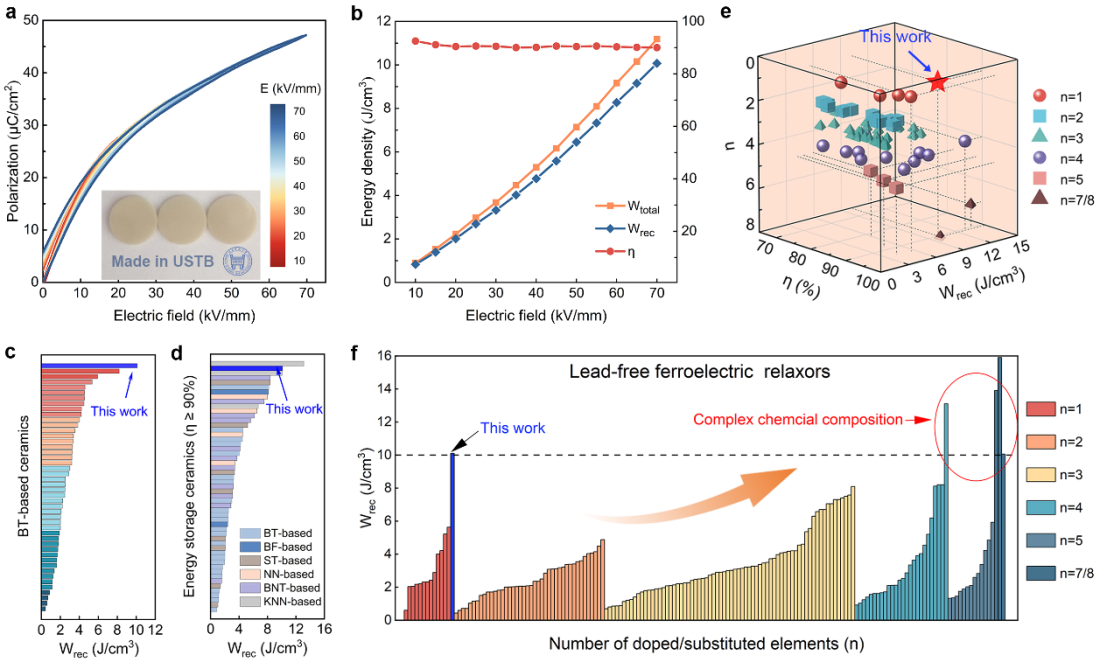

Figure 4. Superior energy storage properties of BBT12 ceramic. (a) Unipolar P-E loops for measured till the maximum applied electric field. The inset indicates the prepared high-quality ceramics. (b) W_{total}, W_{rec}, and η as a function of electric field. (c) A comparison of W_{rec} in BT-based ceramics. (d) A comparison of W_{rec} in these lead-free ceramics with η ≥ 90%. (e) and (f) A multi-dimensional comparison including chemical composition, W_{rec} and η of high-performance ceramics in lead-free ferroelectric relaxor ceramics.

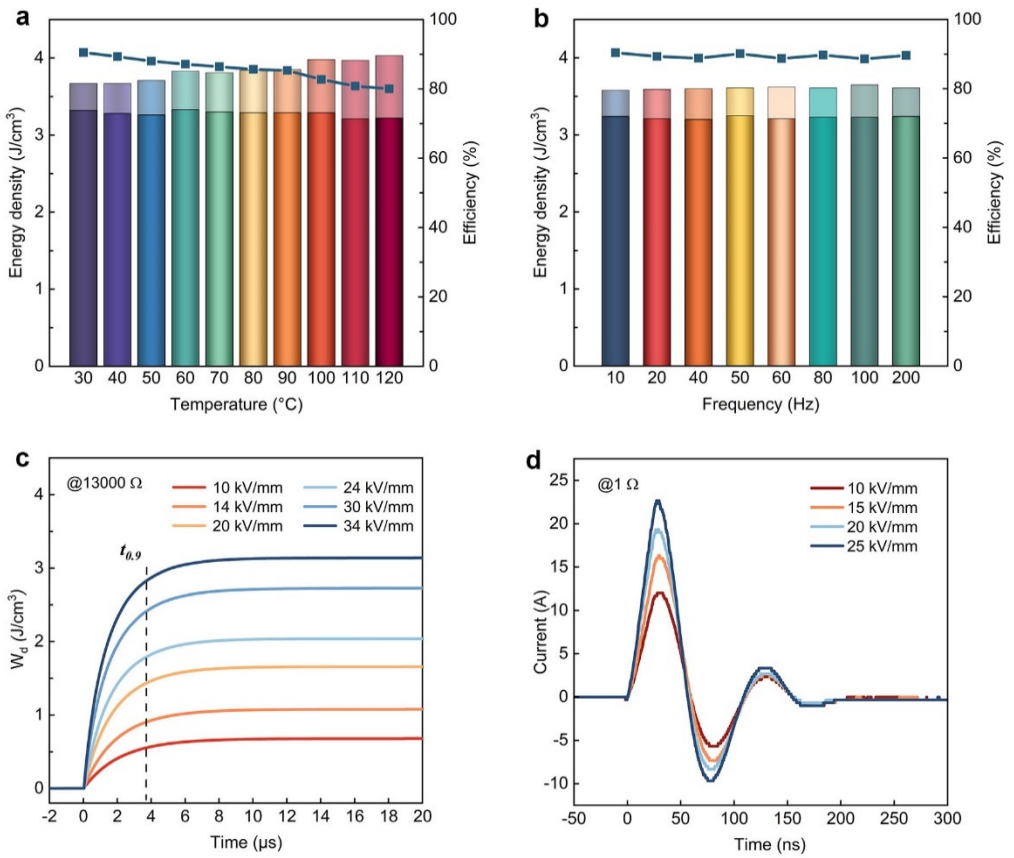

Figure 5. Stability and charge/discharge performance of BBT12 ceramic. (a) Temperature-dependent and (b) frequency-dependent of energy density and energy storage efficiency. (c) Overdamped (R = 13000 Ω) discharge energy density current curves, and (d) underdamped (R = 1Ω) discharge current curves.

BBT exhibits excellent thermal and frequency stability under electric field of 30 kV/mm (Figs. 5(a-b) and S9). In the range of 20-120 °C, BBT maintains high energy storage performance of W_{rec} ~ 3.28±0.07 J/cm^3 with η ~ 85.57±5.57%. Simultaneously, BBT exhibits extremely high-frequency stability in the range of 10-200 Hz, with W_{rec}~3.23±0.03 J/cm^3, η~90.1±1%. It is of great significance to maintain stable energy storage performance at different temperatures/frequencies, which is beneficial to meet the needs of most application scenarios. Another core parameter for practical applications is the charge-discharge performance. The overdamped (R =13000 Ω) discharge test results demonstrate that the ultra-high discharge energy density (W_d =3.13 J/cm^3) is completed in an ultrafast time ($t_{0.9}$ = 3.7 μs) under 34 kV/mm (Fig. 5c). The electric field dependent underdamped (R= 1 Ω) discharge current curve is smooth

and stable, representing a stable discharge performance (Fig. 5d). Ultrahigh current density (C_D = 2386 A/cm^2) and power density (P_D = 298 MW/cm^3) is obtained under 25 kV/mm. The ultrafast and stable discharge rate demonstrates the potential practical application of BBT.

BBT12 ceramic presents superior energy storage density and efficiency together with excellent thermal & frequency stability and excellent charge/discharge properties, thus showing very promising for advanced high-power applications. The excellent properties should be attributed to the large ΔP from the enhanced P_m and reduced P_r, and the minimized hysteresis, as well as the large E_b (Fig. S10). The large ΔP arises from strong local polar fluctuations, owing to the localized Bi with its $6s^2$ strongly hybridizing with the O $2p$ orbitals. The minimized hysteresis and frequency-insensitive polarization response can be ascribed to the slush-like structure with extremely small polar clusters that can facilitate the polar rotation and extension with respect to the electric field. The improved E_b can ascribe to the following facts: the raw material Bi_2O_3 act as a sintering additive, enabling the ceramics to sinter with fine-grain and high-density (Fig. 2a), which can also be manifested in the measured ultrahigh Vickers hardness (H_v = 8.25 GPa) (Fig. S11). The high quality of the ceramics leads to a narrow distribution of E_b data (Fig. S12c). BBT12 presents a much smaller grain size compared with previously reported $BaTiO_3$-Bi$Me$$O_3$ relaxors[41,42]. This would typically yields high E_b , since the E_b is inversely proportional to the grain sizes[43]. The introduction of Bi leads to a slightly improved E_g (2.85 eV) compared with BT, and meanwhile, the electrical resistivity is significantly improved (Figs. S12(a-b)). It could be the non-equivalent substitution suppresses the generation of oxygen vacancies. All these factors together yield low possibility of intrinsic breakdown[44].

In summary, high energy storage density (10.1 J/cm^3) and efficiency (90%) are obtained simultaneously in BBT12 bulk ceramics with very simple composition, via a judicious design of local structure to yield strong local polar fluctuations. Importantly, the results from the atomic-resolution polar mapping and the 3D reconstruction of nanoscale structure from neutron/X-ray total scattering demonstrate that the local Bi-rich regions

provide a large polar length and disrupt the coherence of $[111]_c$ preferred Ti polar displacement. Such mismatched polar displacement results in slush-like polar clusters with extremely small size and strong fluctuation, which ultimately leads to largely improved polarization and vanished hysteresis under high electric field macroscopically. Concurrently, the material exhibits excellent thermal stability (RT-120 °C), with minimal variations less than 2 and 5% for W_{rec} and η, respectively), and extremely high frequency stability. The merits for energy storage properties combined with simple chemical composition demonstrate that BBT12 is a promising candidate of high-power energy storage applications, plus that BT-based materials is the most important commercially used dielectric capacitors. This work breaks through the current situation where high energy storage performance requires very complex chemical components, and offers a feasible avenue to chemical design of new relaxors for high-performance capacitive energy storage.

ACKNOWLEDGMENTS

This work was supported by the National Natural Science Foundation of China (Grant Nos. 22075014, 21825102, and 22235002), the Fundamental Research Funds for the Central Universities, China (Grant No. 06500162), the China Postdoctoral Science Foundation (BX20200044, 2020M680344). A portion of this research used resources at the Spallation Neutron Source, a DOE Office of Science User Facility operated by the Oak Ridge National Laboratory. The use of the Advanced Photon Source at Argonne National Laboratory was supported by the U. S. Department of Energy, Office of Science, Office of Basic Energy Sciences, under Contract No. DE-AC02-06CH11357.

References

[1] Pan H. et al. Ultrahigh energy storage in superparaelectric relaxor ferroelectrics. *Science* **374**, 100–104 (2021).
[2] Kim J. et al. Ultrahigh capacitive energy density in ion-bombarded relaxor ferroelectric films. *Science* **369**, 81–84 (2020).
[3] Li, J. et al. Grain-orientation-engineered multilayer ceramic capacitors for energy storage applications. *Nat. Mater.* **19**, 999–1005 (2020).
[4] Wang G. et al. Electroceramics for High-Energy Density Capacitors: Current Status and Future

Perspectives. *Chem. Rev.* **121**, 6124−6172 (2021).
[5] Yang L., Kong X., Li F., Hao H., Cheng Z., Liu H., Li J.-F. & Zhang S. Perovskite lead-free dielectrics for energy storage applications. *Prog. Mater. Sci.* **102**, 72–108 (2019).
[6] Yao Z. et al. Homogeneous/inhomogeneous-structured dielectrics and their energy-storage performances. *Adv. Mater.* **29**, 1601727 (2017).
[7] Wei X.-K. et al. Progress on Emerging Ferroelectric Materials for Energy Harvesting, Storage and Conversion. *Adv. Energy Mater*. **12**, 2201199 (2022).
[8] Hu D. et al. Optimization the energy density and efficiency of $BaTiO_3$-based ceramics for capacitor applications. *Chem. Eng. J.* **409**, 127375 (2021).
[9] Li J., Li F., Xu Z. & Zhang S. Multilayer lead-free ceramic capacitors with ultrahigh energy density and efficiency. *Adv. Mater.* **30**, 1802155 (2018).
[10] Yao F.-Z. et al. Multiscale structural engineering of dielectric ceramics for energy storage applications: from bulk to thin films. *Nanoscale* **12**, 17165-17184 (2020).
[11] Ji H. et al. Ultrahigh energy density in short-range tilted NBT-based lead-free multilayer ceramic capacitors by nanodomain percolation, *Energy Storage Materials* **38,** 113–120 (2021).
[12] Yang Z., Du H., Jin L.& Poelman D. High-performance lead-free bulk ceramics for electrical energy storage applications: design strategies and challenges. *J. Mater. Chem. A* **9**, 18026-18085 (2021).
[13] Li S. et al. Giant energy density and high efficiency achieved in silver niobate-based lead-free antiferroelectric ceramic capacitors via domain engineering. *Energy Storage Materials* **34,** 417–426 (2021).
[14] Cui T., Zhang J., Gu J., Li X., Guo S., Huan Y., Wang J., Zhang S.-T. & Wang Y. Outstanding comprehensive energy storage performance in lead-free $BiFeO_3$-based relaxor ferroelectric ceramics by multiple optimization design. *Acta Mater.* **240**, 118286 (2022).
[15] Hu Q. et al. Achieve ultrahigh energy storage performance in $BaTiO_3$–$Bi(Mg_{1/2}Ti_{1/2})O_3$ relaxor ferroelectric ceramics via nano-scale polarization mismatch and reconstruction. *Nano Energy* **67**, 104264 (2020).
[16] Zuo, C. et al. Excellent energy storage and hardness performance of $Sr_{0.7}Bi_{0.2}TiO_3$ ceramics fabricated by solution combustion-synthesized nanopowders. *Chem. Eng. J.* **442,** 136330 (2022).
[17] Yan F. et al. Significantly enhanced energy storage density and efficiency of BNT-based perovskite ceramics via A-site defect engineering. *Energy Storage Materials* **30**, 392–400 (2020).
[18] Pan H. et al. Ultrahigh–energy density lead-free dielectric films via polymorphic nanodomain design. *Science* **365**, 578–582 (2019).
[19] Qi H., Xie A., Tian A. & Zuo R. Superior energy-storage capacitors with simultaneously giant energy density and efficiency using nanodomain engineered $BiFeO_3$-$BaTiO_3$-$NaNbO_3$ lead-free bulk ferroelectrics. *Adv. Energy Mater.* **10**, 1903338 (2020).
[20] Chen L., Wang N., Zhang Z., Yu H., Wu J., Deng S., Liu H., Qi H. & Chen J. Local diverse polarization optimized comprehensive energy-storage performance in lead-free superparaelectrics. *Adv. Mater.* **34**, 2205787 (2022).
[21] Xie A. et al. Supercritical relaxor nanograined ferroelectrics for ultrahigh-energy-storage capacitors. *Adv. Mater.* **34**, 2204356 (2022).
[22] Chen L., Deng S., Liu H., Wu J., Qi H. & Chen J. Giant energy-storage density with ultrahigh efficiency in lead-free relaxors via high-entropy design. *Nat. Commun.* **13,** 3089 (2022).
[23] Luo N. et al. Constructing phase boundary in $AgNbO_3$ antiferroelectrics: pathway simultaneously achieving high energy density and efficiency. *Nat. Commun.* **11**, 4824 (2020).
[24] Gao J. et al. Enhanced antiferroelectric phase stability in La-doped $AgNbO_3$: perspectives from the microstructure to energy storage properties. *J. Mater. Chem. A* **7**, 2225-2232 (2019).
[25] Zhu C., Cai Z., Luo B., Guo L., Li L. & Wang X. High temperature lead-free BNT-based ceramics with stable energy storage and dielectric properties. *J. Mater. Chem. A* **8**, 683-692 (2020).
[26] Lu Z. et al. Mechanism of enhanced energy storage density in $AgNbO_3$-based lead-free antiferroelectrics. *Nano Energy* **79**, 105423 (2021).
[27] Qi H. et al. Ultrahigh energy-Storage density in $NaNbO_3$-based lead-free relaxor antiferroelectric ceramics with nanoscale domains. *Adv. Funct. Mater.* **29**, 1903877 (2019).
[28] Yang W. et al. Superior energy storage properties in $NaNbO_3$-based ceramics via synergistically optimizing domain and band structures. *J. Mater. Chem. A* **10**, 11613-11624 (2022).
[29] Zhao L., Liu Q., Gao J., Zhang S. & Li J.-F. Lead-free antiferroelectric silver niobate tantalate

with high energy storage performance. *Adv. Mater.* **29**, 1701824 (2017).
[30] Yang H. et al. Novel $BaTiO_3$-Based, Ag/Pd-compatible lead-free relaxors with superior energy storage performance. *ACS Appl. Mater. Inter.* **12**, 43942–43949 (2020).
[31] Zhou M., Liang R., Zhou Z. & Dong X. Combining high energy efficiency and fast charge-discharge capability in novel $BaTiO_3$-based relaxor ferroelectric ceramic for energy-storage. *Ceram. Int.* **45,** 3582–3590 (2019).
[32] Choi, S. W. et al. Dielectric and pyroelectric properties in the $Pb(Mg_{1/3}Nb_{2/3})O_3$–$PbTiO_3$ system. *Ferroelectrics* **100**, 29–38 (1989).
[33] Liu L, Ren S, Zhang J, Peng B, Fang L, Wang D. Revisiting the temperature-dependent dielectric permittivity of Ba $(Ti_{1x}Zr_x)O_3$. J Am Ceram Soc. 2018;101:2408–2416.
[34] Takenaka, H., Grinberg, I., Liu, S. & Rappe, A. M. Slush-like polar structures in single-crystal relaxors. *Nature* **546**, 391–395 (2017).
[35] Bencan, A., Oveisi, E., Hashemizadeh, S. et al. Atomic scale symmetry and polar nanoclusters in the paraelectric phase of ferroelectric materials. Nat Commun 12, 3509 (2021).
[36] Egami, T.; Billinge, S. J. L. Underneath the Bragg Peaks:Structural Analysis of Complex Materials; Pergamon Press: Oxford, 2003
[37] David A. Keen (2020) Total scattering and the pair distribution function in crystallography, Crystallography Reviews, 26:3, 143-201
[38] Tucker, M. G.; Keen, D. A.; Dove, M. T.; Goodwin, A. L.; Hui, Q. RMCProfile: reverse Monte Carlo for polycrystalline materials. J. Phys.: Condens. Matter 2007, 19, No. 335218.
[39] Eremenko, M.; Krayzman, V.; Bosak, A.; Playford, H. Y.;Chapman, K. W.; Woicik, J. C.; Ravel, B.; Levin, I. Local atomic order and hierarchical polar nanoregions in a classical relaxor ferroelectric. Nat. Commun. 2019, 10, 2728.
[40] Cui T. et al. Simultaneous achievement of ultrahigh energy storage density and high efficiency in BiFeO3-based relaxor ferroelectric ceramics via a highly disordered multicomponent design. *J. Mater. Chem. A* **10**, 14316-14325 (2022).
[41] Jiang X. et al. Enhanced energy storage and fast discharge properties of $BaTiO_3$ based ceramics modified by $Bi(Mg_{1/2}Zr_{1/2})O_3$. *J. Eur. Ceram. Soc.* **39**, 1103–1109 (2019).
[42] Yi X. et al. Effects of sintering method and $BiAlO_3$ dopant on dielectric relaxation and energy storage properties of BaTiO3–BiYbO3 ceramics. *Phys. Status Solidi A* **217**, 1900721 (2020).
[43] Zhang M. et al. Significant increase in comprehensive energy storage performance of potassium sodium niobate-based ceramics via synergistic optimization strategy. *Energy Storage Materials* **45**, 861–868 (2022).
[44] Li D. et al. Improved Energy Storage Properties Achieved in (K, Na)NbO_3-Based Relaxor Ferroelectric Ceramics via a Combinatorial Optimization Strategy. *Adv. Funct. Mater.* **32**, 2111776 (2022).